# Behzad KadkhodaeiElyaderani

Ph.D. student in Mechanical Eng. Univ. of Maryland, College Park

## Joshua L. Leibowitz

Resident surgeon, Univ. of Maryland School of Medicine

# Yejin Moon

Ph.D. student in Mechanical Eng. Univ. of Maryland, College Park

# **Stephen Stachnik**

Resident surgeon, Univ. of Maryland School of Medicine

### **Morcos Awad**

Resident surgeon, Univ. of Marvland School of Medicine

# Grace M. Sarkar

Undergraduate researcher, Univ. of Maryland, College Park

### Anna E. Shaw

Undergraduate researcher, Univ. of Maryland, College Park

# **Shelby Stewart**

Thoracic surgeon, Univ. of Maryland School of Medicine

# Melissa Culligan

Registered nurse, Temple Univ.

# Joseph S. Friedberg

Thoracic surgeon, Temple Univ.

### Jin-Oh Hahn

Prof. of Mechanical Eng., Univ. of Maryland, College Park

# Hosam K. Fathy

Prof. of Mechanical Eng., Univ. of Maryland, College Park (Corresponding author, hfathy@umd.edu)

# Modeling the Impact of Abdominal Pressure on Hypoxia in Laboratory Swine<sup>1</sup>

This paper presents an experimentally parameterized model of the dynamics of oxygen transport in a laboratory animal that simultaneously experiences: (i) a reduction in inspired oxygen plus (ii) an increase in intra-abdominal pressure. The goal is to model the potential impact of elevated intra-abdominal pressure on oxygen transport dynamics. The model contains three compartments, namely, the animal's lungs, lower body vasculature, and upper body vasculature. The model assumes that intra-abdominal pressure affects the split of cardiac output among the two vasculature compartments and that aerobic metabolism in each compartment diminishes with severe hypoxia. Fitting this model to a laboratory experiment on an adult male Yorkshire swine using a regularized nonlinear least squares approach furnishes both physiologically plausible parameter values plus a reasonable quality of fit.

Keywords: Hypoxia, gas transport dynamics, system identification, regularization

### 1 Introduction

This paper models the potential coupling between two physiological phenomena, namely: (i) elevated intra-abdominal pressure and (ii) hypoxia. The paper examines a laboratory animal whose oxygen supply is reduced to induce hypoxia, or deficiency in blood oxygen concentration. Suppose the pressure in this animal's abdomen, known as intra-abdominal pressure (IAP), is elevated. The paper's goal is to examine and model the degree to which this elevated IAP potentially affects the dynamics of hypoxia.

At least two factors motivate the above research question. First, there is a need to provide life support for patients with respiratory failure due to ailments such as COVID-19. Even prior to the COVID-19 pandemic, more than 100,000 patients were hospitalized annually in the United States alone due to respiratory failure [1]. Second, the literature suggests that it may be possible to use oxygen carriers, such as perfluorocarbons (PFCs) or oxygen microbubbles (OMBs), to deliver oxygen to patients or laboratory animals experiencing respiratory distress [2–4]. Different pathways exist for perfusing (or circulating) these oxygen carriers through the body, including peritoneal and enteral perfusion [5–10]. This paper focuses on *peritoneal oxygenation*, where an

<sup>&</sup>lt;sup>1</sup>Paper presented at the 2023 Modeling, Estimation, and Control Conference (MECC 2023), Lake Tahoe, NV, Oct. 2-5. Paper No. MECC2023-151.

oxygen carrier is perfused through the peritoneal (i.e., abdominal) cavity of a patient or laboratory animal using surgically inserted catheters. The idea is to enable the diffusion-based transport of oxygen through the abdominal tissue into the bloodstream, thereby employing the abdomen as a "third lung" in a manner similar to its use as a "third kidney" during peritoneal dialysis [11]. This creates a critical tradeoff: on the one hand, one can plausibly hypothesize that more aggressive perfusion conditions (e.g., higher perfusion flowrates and pressures) have the potential to improve the effectiveness of gas transport during peritoneal oxygenation. On the other hand, elevated perfusion pressures, or IAPs, are known to cause adverse conditions such as intra-abdominal hypertension (IAH) and abdominal compartment syndrome (ACS) [12]. This makes it important to examine and model the potential coupling between IAP on the one hand and the dynamics of hypoxia on the other hand. The overarching goal of this paper is to model this coupling using data from a laboratory experiment on an adult male Yorkshire swine.

There is a rich existing literature on the modeling of gas transport dynamics, including both oxygen and carbon dioxide transport, in both human patients and laboratory animals [13–20]. Previous work by the authors also examines the problem of modeling cavity pressure dynamics in adult male Yorkshire swine [21]. However, to the best of the authors' knowledge, modeling the coupling between cavity pressure and hypoxia dynamics remains relatively unexplored in the literature.

This paper presents three novel contributions to the literature, collectively addressing the above gap.

- First, the paper presents a model for the coupling between cavity pressure and the dynamics of hypoxia in laboratory swine. The model assumes this coupling to be unidirectional, meaning that cavity pressure affects the dynamics of hypoxia, but not vice versa. In fact, our prior experiments (including the one used in this paper) showed that hypoxia without PFC perfusion never produced a statistically significant changes in IAP, thus justifying our assumption. Fig. 1 presents a simple schematic of this three-compartment model, where the compartments are the lungs, the upper body vasculature, and the lower body vasculature. The model assumes that a particular set of underlying mechanisms governs the coupling between IAP and the dynamics of hypoxia. The intent of the model is neither to prove nor disprove these governing mechanisms, but rather to examine the degree to which these assumed mechanisms may potentially fit experimental data from tests on laboratory swine. Specifically, the model assumes that when intra-abdominal pressure is elevated by a significant degree, the flow of blood from the animal's lower body back to the heart, through the inferior vena cava (IVC) is partially or fully occluded. This occlusion reduces the oxygen available to the animal's lower body, thereby reducing aerobic metabolism in the lower body. In contrast, the animal's upper body vasculature receives a larger fraction of systemic blood flow without occlusion, thereby potentially experiencing a reduction in the severity of hypoxia.
- Second, the paper presents data from a laboratory animal experiment where an adult male Yorkshire swine simultaneously experiences a reduction in the fraction of inspired oxygen (FiO2) plus an increase in IAP. The increase in IAP is sufficiently large to induce ACS, and coincides with an improvement in upper-body pulse oximetry.
- Third, the paper uses nonlinear least squares estimation to
  fit the parameters of the above model to the above experimental dataset. Regularization is utilized to penalize parameter deviations from physiologically plausible nominal values,
  consistent with earlier physiological modeling research by the
  authors [22]. The end result is a model that achieves a good
  quality of fit while remaining physiologically plausible.

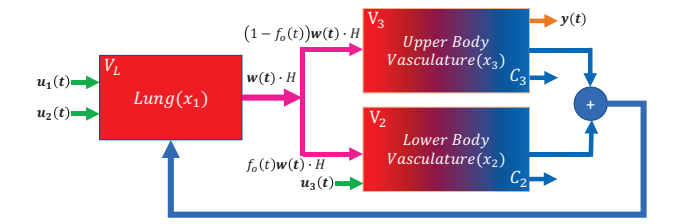


Fig. 1 Schematic of proposed model. The model receives three inputs including minute ventilation  $(u_1)$ , FiO2  $(u_2)$ , and IAP  $(u_3)$  to predict SpO2 in the upper body vasculature (y).

The remainder of this paper is organized as follows. Section 2 summarizes the proposed model. Section 3 presents the perfusion setup used for the paper's animal experiment, and summarizes the results of this experiment. Section 4 presents the parameterization approach used for model fitting, as well as the results of this parameterization. Finally, Section 5 summarizes the paper's conclusions.

### 2 Proposed Model

The proposed model uses three state variables to represent the dynamics of gas transport. The first state variable,  $x_1(t)$ , is the alveolar partial pressure of oxygen in the animal's lung compartment. The remaining state variables,  $x_2(t)$  and  $x_3(t)$ , are the percent oxygen saturations in the animal's lower and upper body vasculature compartments, respectively. The model has three control inputs plus one exogenous input. The first control input  $u_1(t) = MV/60$ , is the animal's inhalation/exhalation rate, or its minute ventilation divided by 60. The second control input,  $u_2(t)$ , is the fraction of inspired oxygen, expressed as a percentage. The third control input,  $u_3(t)$ , is the animal's cavity pressure, or IAP. In animal experiments employing mechanical ventilation plus peritoneal perfusion,  $u_1(t)$  and  $u_2(t)$  can be adjusted by changing the ventilator setting, whereas  $u_3(t)$  can be adjusted through perfusion control. The exogenous input, w(t), is the animal's cardiac output in liters per second. Finally, the model's main output, y(t), is pulse oximetry (SpO2), or the percentage of oxygen saturation in the animal's arteries. The proposed model assumes that this saturation percentage can be computed from the alveolar partial pressure of oxygen, which is used as an approximation of the partial pressure of oxygen in the pulmonary veins and systemic arteries. This computation is performed using the Hill equation [23]:

$$y = f_d(x_1) = 100 \frac{(x_1/p_o)^r}{1 + (x_1/p_o)^r}$$
 (1)

where the Hill function  $f_d$  represents the hemoglobin dissociation curve,  $p_o$  is the partial pressure of oxygen at 50% pulse oximetry, and r is a constant governing the steepness of the dissociation curve.

The proposed model makes three key assumptions regarding the impact of peritoneal perfusion on the dynamics of hypoxia. First, the model neglects the diffusion of oxygen from the perfusate to the animal's bloodstream, even if the perfusate is an oxygen carrier. The idea is to focus this modeling effort entirely on the potential impact of perfusion pressure on the dynamics of hypoxia, leaving the problem of modeling oxygen diffusion from the perfusate into the bloodstream open for future research. Second, the model assumes that the fraction of total cardiac output circulating through the lower body vasculature is given by some function,  $f_o(u_3(t))$ . This function is tailored to model the occlusion of venous return from the lower body, through IVC, at high perfusion pressures. Finally, the model assumes that metabolism in each body compartment is related to the corresponding oxygen saturation percentage through some function  $f_m(x_i)$ , where i is the index of the compartment and the function  $f_m$  is tailored to represent a switch to anaerobic metabolism at very low oxygen saturations. Both of the above two functions are selected to be sigmoidal, as shown below:

$$f_o(u_3) = \frac{1}{1 + (u_3/p^*)^{r^*}} \frac{V_2}{V_2 + V_3}, \quad f_m(x_i) = \frac{(x_i/p_m)^{r_m}}{1 + (x_i/p_m)^{r_m}}$$
 (2)

where  $V_2$  is the volume of the lower vasculature compartment ending in IVC,  $V_3$  is the volume of the upper vasculature compartment ending in the superior vena cava,  $p^*$  is an IAP value governing the onset of venous return occlusion,  $r^*$  is a constant describing the steepness of the impact of IAP on occlusion,  $p_m$  is a percentage oxygen saturation governing the onset of anaerobic metabolism, and  $r_m$  is a constant describing the steepness of this onset.

Given the above definitions, the proposed model is governed by the following state equations:

$$\begin{split} \frac{V_L}{760} \dot{x}_1 &= u_1 \left[ \frac{u_2}{100} - \frac{x_1}{760} \right] \\ &+ \frac{wH}{100} \left[ f_o(u_3)(x_2 - f_d(x_1)) \\ &+ (1 - f_o(u_3))(x_3 - f_d(x_1)) \right] \\ \frac{HV_2}{100} \dot{x}_2 &= \frac{wH \left[ f_o(u_3)(f_d(x_1) - x_2) \right]}{100} - f_m(x_2) V_2 C \\ \frac{HV_3}{100} \dot{x}_3 &= \frac{wH \left[ (1 - f_o(u_3))(f_d(x_1) - x_3) \right]}{100} - f_m(x_3) V_3 C \end{split}$$
(3)

where  $V_L$  is lung volume, H is the (dimensionless) maximum solubility of oxygen in the animal's blood [24], and C is the animal's maximum aerobic oxygen consumption rate per unit volume of the two vasculature tissues (i.e., the consumption rate corresponding to normoxia).

Each term in the above state-space model represents a volumetric rate of oxygen transport, consumption, or accumulation, in liters per second. The left hand sides of the state equations represent rates of change of the total amount of oxygen stored in each compartment. The terms on the right hand sides of the state equations that are pre-multiplied by either  $u_1(t)$  or w(t) represent oxygen transport rates due to either breathing or blood flow, respectively. Multiplying cardiac output, w(t), by  $f_o(u_3(t))$  or  $1 - f_o(u_3(t))$  furnishes the volumetric flowrate of blood through either the lower or upper body vasculature compartment, respectively. Finally, the expression  $C_i = f_m(x_i)V_iC$  represents the rate of oxygen consumption in compartment i due to aerobic metabolism, taking into account the curtailment of aerobic metabolism under severe hypoxia.

# 3 Animal Experiment

The authors have conducted 13 animal experiments to date on the "third lung" concept, all of them on adult Yorkshire swine. This paper uses the results from animal experiment #8 to parameterize the above model. An adult Yorkshire swine was intubated and placed on a mechanical ventilator. The animal's fraction of inspired oxygen was reduced in order to induce hypoxia. Minute ventilation remained relatively steady throughout the experiment, as shown in Fig. 2. Hypoxia was induced through a significant reduction in FiO2, followed by an increase in FiO2 at the end of the experiment to allow the animal to recover, as shown in Fig. 3. High IAPs were induced using the peritoneal perfusion of an oxygenated mix of cis- and trans-perfluorodecalin. While it is reasonable to expect the perfusion of this oxygen carrier to result in some oxygen transport into the animal's bloodstream, the IAP reached during this perfusion episode is potentially high enough to cause occlusion of venous return from the animal's lower body, as shown in Fig. 4. Cardiac output experiences a fairly small (negative) change during this experiment, as shown in Fig. 5. Together, these experimental conditions resulted in a rapid decline in pulse

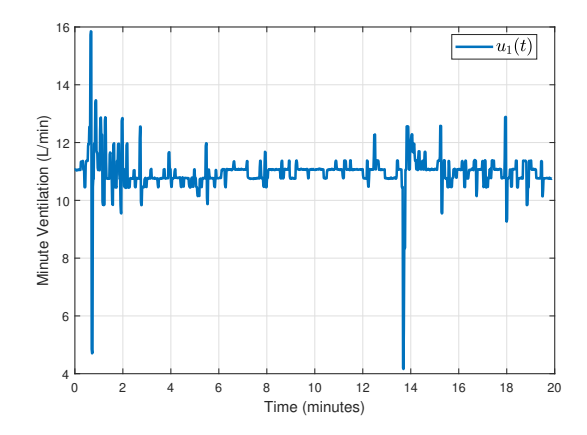


Fig. 2 Minute ventilation during animal experiment

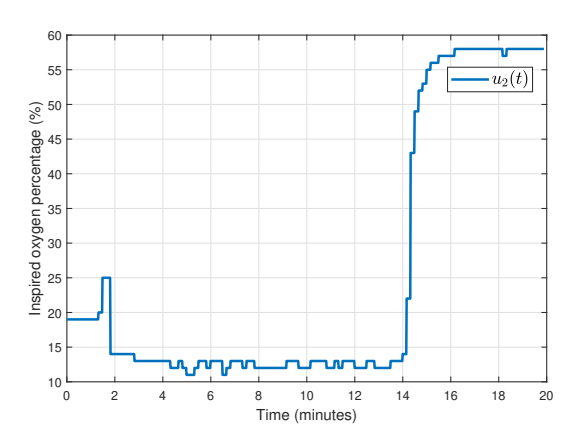


Fig. 3 Inspired oxygen fraction during animal experiment

oximetry, followed by rapid recovery, rapid decline, and final recovery, as shown in Fig. 6. This paper is, in a sense, a dynamic model-based exploration of the possibility that the intermediate recovery and drop in pulse oximetry may potentially be attributable to the corresponding high values of IAP.

### 4 Model Parameterization

The above experimental dataset was used for estimating the parameters of the proposed dynamic model. Thirteen model parameters were optimized, as listed in Table 1. In this table,  $V_b = V_2 + V_3$  is the animal's total blood volume, and  $V_{ratio} = V_2/V_b$  is the fraction of this total volume occupying the lower body vasculature. We estimated the bounds on  $V_{ratio}$  based on the values reported in the literature for blood flowrates in the superior versus inferior vena

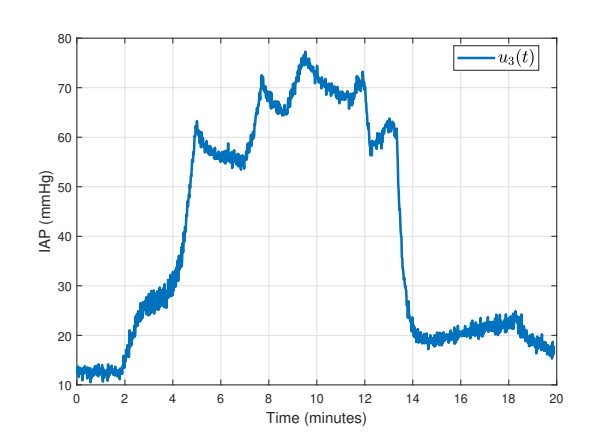


Fig. 4 IAP during animal experiment

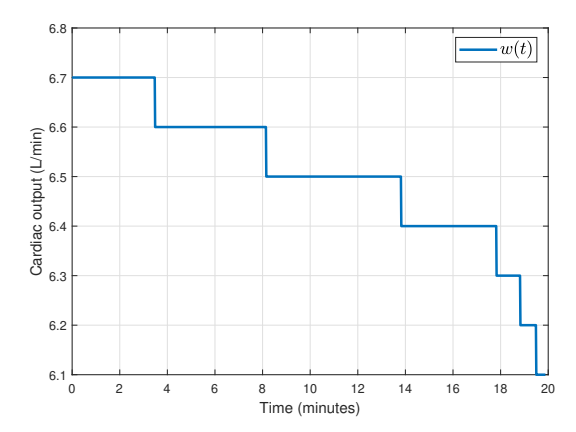


Fig. 5 Cardiac output during animal experiment

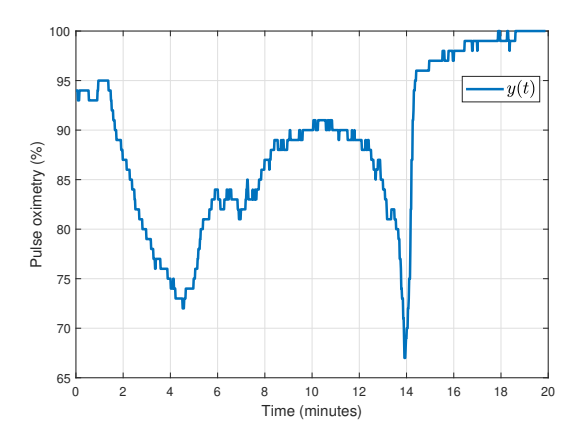


Fig. 6 Pulse oximetry during animal experiment

cava, assuming these flowrates to be proportional to the volumes of the corresponding vasculature compartments [25,26]. Optimization encompassed both constant model parameters and the initial conditions for the three state variables, with the initial conditions for  $x_2$  and  $x_3$  assumed to be equal. Optimization was performed using the Matlab implementation of the particle swarm evolutionary optimizer. The optimization objective was a linearly weighted summation of two Pareto objectives:

$$J = w_p J_{reg}^2 + (1 - w_p) J_{fit}^2$$
 (4)

where  $J_{fit}$  is the root mean square error for the prediction of pulse oximetry over the duration of the fitting experiment, and  $J_{reg}$  is a regularization penalty function. The intent of this penalty function is to avoid potential practical model identifiability issues and simultaneously to ensure the physiological plausibility of the model parameter estimates. Specifically, for each parameter,  $\theta_i$ , where i=1,...,13, Table 1 provides a reasonable nominal value plus a lower bound and an upper bound. Given an estimate of each parameter,  $\hat{\theta}_i$ , one can compute the following regularization penalty:

$$J_{i} = \left[\frac{\hat{\theta}_{i} - \theta_{i,nom}}{\theta_{i,ub} - \theta_{i,lb}}\right]^{2} \tag{5}$$

The overall regularization penalty is then given by:

$$J_{reg} = \sum_{i=1}^{13} J_i + \left[ \frac{0.009 - \theta_2 \theta_6}{0.002} \right]^2$$
 (6)

where the final term in the above equation penalizes the deviation of  $\theta_2\theta_6 = V_BC$ , from a target value of the total normoxic oxygen

Table 1 Parameter estimation settings/results

No.	Coeff.	Unit	Optimal	Nominal	Min	Max	Ref.
1	$V_L$	Liter	2.72	2.28	1	5	[27]
2	$V_b$	Liter	3.49	3.42	1	8	[28]
3	$V_{ratio}$	_	0.7	0.5	0.3	0.7	[25]
4	$r_m$	_	4.42	4	1.5	6	-
5	$r^*$	_	7.0	2.3	2	7	-
		$L O_2$					
6	C	$\frac{s}{L \ blood}$	31e-4	15e-4	5e-4	4e-3	[29]
7	$p_o$	mmHg	35.98	29	15	45	[23]
8	r	_	2.51	2.3	1.5	3.5	[23]
9	$p_m$	%	5.0	40	5	60	[13]
10	$p^*$	mmHg	47.79	30	10	80	$u_3$
11	$x_{1,init}$	mmHg	100.06	120	60	200	[30]
12	$x_{2,3,init}$	%	74.09	90	40	95	[31]
13	H	_	0.19	0.2	0.15	0.35	[24]

consumption rate of the animal, in liters of oxygen per second. This target value, equal to 540mL of oxygen per minute, was estimated based on an average measured minute ventilation rate of 11 liters per minute plus an average measured difference of 5% between inspired and end-tidal oxygen.

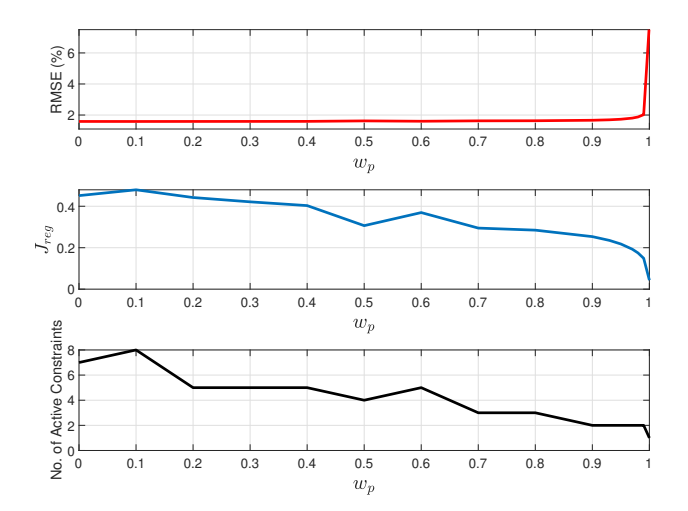


Fig. 7 Pareto analysis plot

The solution of the above problem depends on the weight,  $w_p$ . Fig. 7 summarizes 16 different potential solutions for different values of this weight. The three subfigures (from top to bottom) show the root mean square error for percentage pulse oximetry prediction, the values of the regularization cost, and the number of active constraints for each of these trials. It is difficult to compute the number of active constraints exactly when using an evolutionary optimization algorithm, such as particle swarm optimization. With this in mind, any bound on a parameter  $\theta_i$  is deemed approximately active in Fig. 7 if the normalized value of the parameter,  $(\theta_i - \theta_{i,lb})/(\theta_{i,ub} - \theta_{i,lb})$ , falls outside the range [0.05, 0.95]. The plot suggests that a value  $w_p = 0.93$  of the weight on the regularization penalty achieves a very reasonable root mean square prediction error, with only a small number of approximately active constraints. Noting that  $J_{reg}$  and  $J_{fit}$  are not scaled relative to each other, the value of this regularization weight does not necessarily imply that 93% of the total emphasis in optimization is placed on regularization, but is rather at least partially a reflection of the relative magnitudes of the competing optimization objectives. Table 1 lists the optimal parameter values corresponding to this regularization weight. A small number of parameters hit the bound:  $V_{ratio}$ ,  $r^*$ , and  $p_m$ . However, given that all the parameter

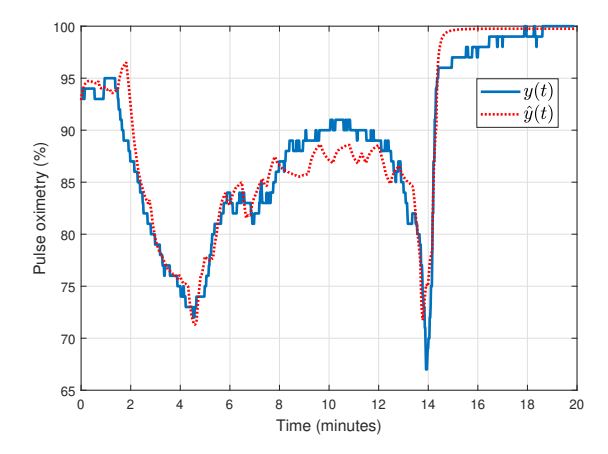


Fig. 8 Comparison between modeled  $(\hat{y}(t))$  and measured (y(t)) pulse oximetry

bounds were defined based on the data available in the literature, their values were still acceptable.

Fig. 8 compares the measured pulse oximetry from the animal experiment to the predictions of the proposed model. The model fits the experimental data reasonably well, with the important note that relaxing the regularization penalty has the potential to furnish even better fitting results at the expense of greater departures from the assumed nominal parameter values. Fig. 9 explains these results by showing the predicted fraction of total cardiac output to the lower body vasculature. The proposed model hypothesizes that this fraction diminishes significantly as IAP increases. Finally, Fig. 10 plots the resulting oxygen saturation levels in the two vasculature compartments versus time. When IVC occlusion occurs, oxygen saturation in the lower body vasculature diminishes considerably. This, in turn, causes the lower body vasculature's aerobic metabolism to diminish. The upper body vasculature, in contrast, receives a larger proportion of total cardiac output, resulting in a significant improvement in the corresponding oxygen saturation. Interpreting both of these saturation values as representing venous return, the oxygen saturation in the upper body vasculature is reasonable. The end result is an improvement in the animal's pulse oximetry, driven by the fact that the animal's lungs see venous return predominantly from the upper body.

Despite the promising results, the model presented in this paper has a few limitations, which must be investigated in future work. First, we assumed that upper body and lower body vasculatures are balanced (i.e., larger compartment carries larger cardiac output). This is an intuitively appealing assumption, but it was not strictly validated. Second, we assumed that the vasculature volumes are constant. This allowed us to derive a simple model with a reasonable goodness of fit to the data. But, it may not be strictly valid considering the venous compliance. The ultimate validity of these assumptions must be investigated in future work. Third, the model results related to shunting of cardiac output was not directly corroborated with appropriate sensor measurements. In fact, a subset of the sensors stopped providing meaningful measurements under very high IAPs, making it very difficult to obtain direct evidence for the model results. Future work must experimentally examine the extent to which the model results are realistic.

### 5 Summary and Conclusion

The main conclusion of this paper is that it is possible to fit a physiologically plausible model to animal pulse oximetry data for a combined hypoxia/perfusion experiment with reasonable accuracy. The model is grounded in the hypothesis that elevating IAP to a sufficient degree can potentially occlude venous return through IVC. This increases the fraction of total cardiac output seen by the upper body vasculature, thereby improving overall animal pulse oximetry. It is very important to note that this is only one

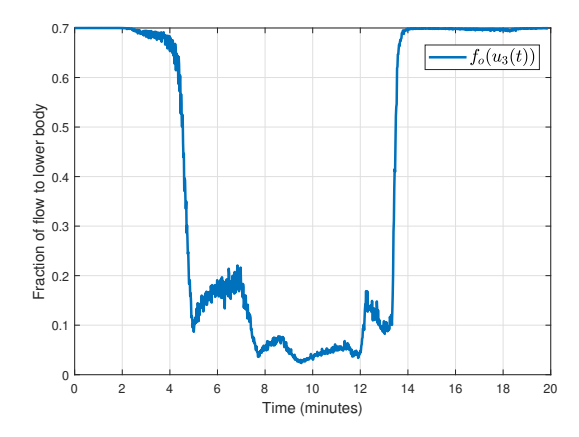


Fig. 9 Lower body fraction of cardiac output

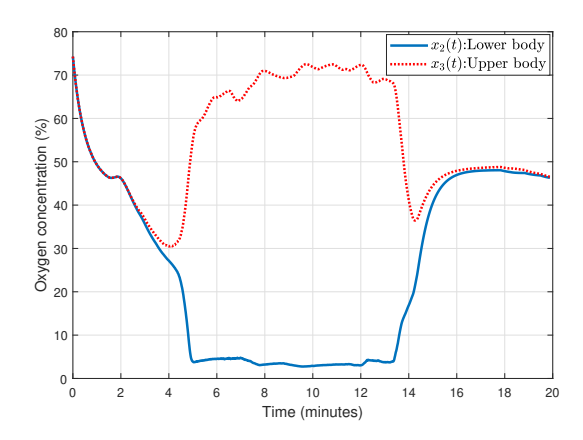


Fig. 10 Predicted oxygen saturations in the vasculature

potential explanatory mechanism for the observed improvement in pulse oximetry in this work's animal experiment. The intent of this work is neither to completely prove nor disprove this mechanism, and it is important to recognize that other mechanisms are likely to be at play, including diffusion-based gas transport. However, it is also interesting to note the degree to which a simple multicompartment model constructed around this mechanism is able to fit the observed improvements in animal pulse oximetry.

### Acknowledgment

Support for this research was provided by the National Science Foundation's Growing Convergence Research (GCR) program under Grants OIA2121110 and OIA2227939. The authors gratefully acknowledge this support.

### References

- Eworuke, E., Major, J. M., and McClain, L. I. G., 2018, "National incidence rates for acute respiratory distress syndrome (ARDS) and ARDS cause-specific factors in the United States (2006–2014)," Journal of critical care, 47, pp. 192– 197.
- [2] Spiess, B. D., 2019, "Perfluorocarbon gas transport: an overview of medical history with yet unrealized potentials," Shock, 52(1S), pp. 7–12.
- [3] Bialas, C., Moser, C., and Sims, C. A., 2019, "Artificial oxygen carriers and red blood cell substitutes: A historic overview and recent developments toward military and clinical relevance," Journal of Trauma and Acute Care Surgery, 87(1S), pp. S48–S58.
- [4] Feshitan, J. A., Legband, N. D., Borden, M. A., and Terry, B. S., 2014, "Systemic oxygen delivery by peritoneal perfusion of oxygen microbubbles," Biomaterials, 35(9), pp. 2600–2606.
- 5] Mohammed, R. U. R., Zollinger, N. T., McCain, A. R., Romaguera-Matas, R., Harris, S. P., Buesing, K. L., Borden, M. A., and Terry, B. S., 2022, "Testing oxygenated microbubbles via intraperitoneal and intrathoracic routes on a large pig model of LPS-induced acute respiratory distress syndrome," Physiological Reports, 10(17), p. e15451.

- [6] Fiala, A., Slagle, C., Legband, N., Aghabaglou, F., Buesing, K., Borden, M., Harris, S., and Terry, B., 2020, "Treatment of a rat model of LPS-induced ARDS via peritoneal perfusion of oxygen microbubbles," Journal of Surgical Research, 246, pp. 450–456.
- [7] Wolfson, M. R. and Shaffer, T. H., 2005, "Pulmonary applications of perfluorochemical liquids: ventilation and beyond," Paediatric respiratory reviews, 6(2), pp. 117–127.
- [8] Carr, S. R., Cantor, J. P., Rao, A. S., Lakshman, T. V., Collins, J. E., and Friedberg, J. S., 2006, "Peritoneal perfusion with oxygenated perfluorocarbon augments systemic oxygenation," Chest, 130(2), pp. 402–411.
- [9] Okabe, R., Chen-Yoshikawa, T. F., Yoneyama, Y., Yokoyama, Y., Tanaka, S., Yoshizawa, A., Thompson, W. L., Kannan, G., Kobayashi, E., Date, H., et al., 2021, "Mammalian enteral ventilation ameliorates respiratory failure," Med, 2(6), pp. 773–783.
- [10] Faithfull, N., Klein, J., Vanderzee, H., and Salt, P., 1984, "Whole body oxygenation using intraperitoneal perfusion of fluorocarbons," British journal of anaesthesia, 56(8), pp. 867–872.
- [11] Doosthosseini, M., Aroom, K. R., Aroom, M. R., Culligan, M., Naselsky, W., Thamire, C., Haslach, H. W., Roller, S. A., Hughen, J. R., Friedberg, J. S., et al., 2022, "Monitoring, control system development, and experimental validation for a novel extrapulmonary respiratory support setup," IEEE/ASME Transactions on Mechatronics, 27(5), pp. 4177–4187.
- [12] Kirkpatrick, A. W., Roberts, D. J., De Waele, J., Jaeschke, R., Malbrain, M. L., De Keulenaer, B., Duchesne, J., Bjorck, M., Leppaniemi, A., Ejike, J. C., et al., 2013, "Intra-abdominal hypertension and the abdominal compartment syndrome: updated consensus definitions and clinical practice guidelines from the World Society of the Abdominal Compartment Syndrome," Intensive care medicine, 39, pp. 1190–1206.
- [13] Mahon, R. T., Ciarlone, G. E., Roney, N. G., and Swift, J. M., 2019, "Car-diovascular parameters in a swine model of normobaric hypoxia treated with 5-hydroxymethyl-2-furfural (5-HMF)," Frontiers in Physiology, 10, p. 395.
- [14] Leach, R. and Treacher, D., 2002, "The pulmonary physician in critical care-2: Oxygen delivery and consumption in the critically ill," Thorax, 57(2), pp. 170–177.
- [15] Kim, C.-S., Ansermino, J. M., and Hahn, J.-O., 2016, "A comparative data-based Modeling study on respiratory CO2 gas exchange during mechanical ventilation," Frontiers in bioengineering and biotechnology, 4, p. 8.
- [16] Doosthosseini, M., Moon, Y., Commins, A., Wood, S., Naselsky, W., Culligan, M. J., Aroom, K., Aroom, M., Shah, A., Bittle, G. J., et al., 2022, "Estimating the Impact of Peritoneal Perfluorocarbon Perfusion on Carbon Dioxide Transport Dynamics in a Laboratory Animal," 2022 American Control Conference (ACC), IEEE, pp. 3000–3005.
- [17] Wood, S., Commins, A., Doosthosseini, M., Naselsky, W., Culligan, M., Aroom, K., Aroom, M., Kadkhodaeielyaderani, B., Moon, Y., Leibowitz, J., et al., 2022, "Experimental Parameterization of a Model of Hypoxia Dynamics in Yorkshire Swine," IFAC-PapersOnLine, 55(37), pp. 752–757.

- [18] Batzel, J. J. and Tran, H. T., 2000, "Stability of the human respiratory control system I. Analysis of a two-dimensional delay state-space model: I. Analysis of a two-dimensional delay state-space model," Journal of mathematical biology, 41, pp. 45–79.
- [19] Batzel, J. J., Kappel, F., Schneditz, D., and Tran, H. T., 2007, Cardiovascular and respiratory systems: modeling, analysis, and control, SIAM.
- [20] Ben-Tal, A. and Tawhai, M. H., 2013, "Integrative approaches for modeling regulation and function of the respiratory system," Wiley Interdisciplinary Reviews: Systems Biology and Medicine, 5(6), pp. 687–699.
- [21] Zaleski, N., Moon, Y., Doosthosseini, M., Hopkins, G., Aroom, K., Aroom, M., Naselsky, W., Culligan, M. J., Leibowitz, J., Shah, A., et al., 2022, "Modeling and Experimental Identification of Peritoneal Cavity Pressure Dynamics During Oxygenated Perfluorocarbon Perfusion," 2022 European Control Conference (ECC), IEEE, pp. 297–302.
- [22] Tivay, A., Jin, X., Lo, A. K.-Y., Scully, C. G., and Hahn, J.-O., 2020, "Practical use of regularization in individualizing a mathematical model of cardiovascular hemodynamics using scarce data," Frontiers in Physiology, 11, p. 452.
- [23] Zhang, J., Nolan, T. D., Zhang, T., Griffith, B. P., and Wu, Z. J., 2007, "Characterization of membrane blood oxygenation devices using computational fluid dynamics," Journal of Membrane Science, 288(1-2), pp. 268–279.
- [24] Stoller, J. K., 2015, "Murray & Nadel's Textbook of Respiratory Medicine," Annals of the American Thoracic Society, 12(8), pp. 1257–1258.
- [25] Salim, M. A., DiSessa, T. G., Arheart, K. L., and Alpert, B. S., 1995, "Contribution of superior vena caval flow to total cardiac output in children: a Doppler echocardiographic study," Circulation, 92(7), pp. 1860–1865.
- [26] Kuzo, R. S., Pooley, R. A., Crook, J. E., Heckman, M. G., and Gerber, T. C., 2007, "Measurement of caval blood flow with MRI during respiratory maneuvers: implications for vascular contrast opacification on pulmonary CT angiographic studies," American Journal of Roentgenology, 188(3), pp. 839–842.
- [27] Parent, R. A., 2015, Comparative biology of the normal lung, Academic Press.
- [28] Bush, J., Jensen, W., Cartwright, G., and Wintrobe, M., 1955, "Blood volume studies in normal and anemic swine," American Journal of Physiology-Legacy Content, 181(1), pp. 9–14.
- [29] Mellon, E. A., Beesam, R. S., Baumgardner, J. E., Borthakur, A., Witschey 2nd, W. R., and Reddy, R., 2009, "Estimation of the regional cerebral metabolic rate of oxygen consumption with proton detected 170 MRI during precision 1702 inhalation in swine," Journal of neuroscience methods, 179(1), pp. 29–39.
- [30] Tyssebotn, I. M., Lundgren, C. E., Olszowka, A. J., and Bergoe, G. W., 2010, "Hypoxia due to shunts in pig lung treated with O2 and fluorocarbon-derived intravascular microbubbles," Artificial Cells, Blood Substitutes, and Biotechnology, 38(2), pp. 79–89.
- [31] Sugiharto, A., Firdausi, R., Safitry, O., et al., 2018, "The effects of declined oxygen levels on hypoxia symptoms and blood gases: An experimental study," *Journal of Physics: Conference Series*, Vol. 1073, IOP Publishing, Paper No. 4, p. 042023.